X

Measurement of the Lunar Neutron Density Profile

Dorothy S. Woolum,* D. S. Burnett,
Marian Furst, and J. R. Weiss

Division of Geological and Planetary Sciences
California Institute of Technology
Pasadena, California 91109

*Also, Physics Department
California State University
Fullerton, California 92631

NAS 9-12585

Contribution No. 2539, Division of Geological and Planetary Sciences, California Institute of Technology

45 pages of manuscript, including 6 figures and 1 table

Abstract

An *in situ* measurement of the lunar neutron density from 20 to 400 g/cm^2 depth between the lunar surface was made by the Apollo 17 Lunar Neutron Probe Experiment (LNPE) using particle tracks produced by the ^{10}B (n,α) ^{7}Li reaction. Both the absolute magnitude and depth profile of the neutron density are in good agreement with theoretical calculations by Lingenfelter, Canfield, and Hampel. However, relatively small deviations between experiment and theory in the effect of Cd absorption on the neutron density and in the relative ^{149}Sm to ^{157}Gd capture rates reported previously (Russ *et al.* 1972) imply that the true lunar ^{157}Gd capture rate is about one half of that calculated theoretically.

I. Introduction

The first round of analyses of the Apollo 11 lunar samples showed that isotopic variations produced by the cumulative long-term neutron exposure of lunar samples could be precisely measured and that the neutron capture effects could be used as a tracer of lunar surface mixing processes (Eugster et al. 1970). Subsequent to this first report, approximately 30 papers have been published concerning neutron capture in lunar materials. Proper interpretation of the lunar sample data requires knowledge of the magnitude of the neutron capture rates and how they vary with depth in the first few meters of the lunar surface. Further, because the neutron capture reactions for different nuclei occur at different energies, some knowledge of the neutron energy spectrum is required to intercompare capture rates for various nuclei. Explicit values for fluxes and/or capture rates as a function of neutron energy and depth have been calculated theoretically by Lingenfelter, Canfield and Hampel (1972; hereafter referred to as LCH), by Armstrong and Alsmiller (1971), and by Kornblum et al. (1973)

The Lunar Neutron Probe Experiment (LNPE) was carried on Apollo 17 in order to put the capture rates and their depth dependence, as nearly as possible, on an experimental basis. The LNPE contained two target-detector systems, both using particle track detectors. We have previously (Woolum and Burnett, 1974a;

hereafter referred to as paper I) published the results of the ^{235}U fission detectors. Excellent agreement was obtained for both the magnitude and depth dependence of the fission rate between the experimental (LNPE) and theoretical (LCH) rates. In this paper, we report the results of the capture rates of ^{10}B, based on the low energy $^{10}B(n,\alpha)\ ^{7}Li$ neutron capture reaction. We shall focus here on the experimental results and the documentation of their accuracy. The implications of the LNPE data for surface mixing processes are discussed in more detail in our paper for the Fifth Lunar Science Conference (Woolum and Burnett, 1974b; hereafter referred to as paper II).

II. Experimental Description

The neutron probe consisted of two, approximately one meter, units which were coupled together and deployed in the drill hole created with the retrieval of the deep core sample. A complete description of the instrument may be found in the Apollo 17 Preliminary Science Report (Woolum et al. 1973).

Each unit of the probe contained a central rod to which the boron targets were bonded. The targets were 1.4 ± 0.2 mg/cm^2 of ^{10}B metal deposited by cracking B_2H_6 at $\sim 800^\circ$ C on half-cylinder-shaped tantalum metal substrates (0.1 mm thick X 76 mm long);

they were mounted essentially continuously on one side of the central rod along the entire two-meter length of the probe. Surrounding each target position on the central rod was an open cylindrical framework (rib cage), around which cellulose triacetate (Triafol TN) plastic detectors were wrapped. These detectors are capable of registering the alpha particles and some of the ^{7}Li recoils emitted in the neutron capture reaction on ^{10}B.

Figure 1 shows a schematic cross-section view of the target-detector geometry. The experimental design was largely dictated by the need for an on-off mechanism which was required to eliminate possible background events produced in flight both by cosmic ray interactions in the spacecraft and by neutrons emitted directly from the PuO_2 power source (the Radioisotope Thermoelectric Generator or RTG) used for the lunar surface geophysical experiments. The activation and deactivation of the LNPE was accomplished manually, with a 180° rotation of the central rod relative to the fixed rib cage. In the activated mode the boron targets faced the mostly open hemisphere of the rib cage, where most of the detector surface area was exposed to the target (Figure 1). In the deactivated mode the targets faced the large support rib of the cage, where only small areas ("windows") of the detectors were exposed at about 4 cm intervals along the length of the probe.

III. Data and Precision

The plastic detector data have been analyzed to determine the neutron density profile. Strips of plastic about 12 mm in length were cut from various positions along the probe; the particle tracks in the plastic were measured at ~ 1000 X magnification using conventional transmitted light, optical scanning techniques, after having been etched for 4.5 hours in a temperature-controlled bath containing 7 parts 6.25 N sodium hydroxide solution and 5 parts 12% sodium hypochlorite solution. The nominal temperature of the bath was 40.2° C; all samples were etched at a temperature within 0.2° C of this value, and for any given sample the temperature of the bath was maintained constant to within 0.1° C.

The data obtained are shown in Figure 2, where the track densities are plotted versus depth beneath the lunar surface. Because of the geometrical configuration of the targets and detectors (see Figure 1), the track density is not uniform over the surface of the detector. The data shown in the figure are the background-corrected, average track densities obtained from a standardized scanning pattern which was fixed for each detector relative to the center of the unexposed "trackless" region behind the small central midrib (Fig 1). This pattern traversed the prime, relatively uniformly irradiated, detector areas indicated in

Figure 1. The overall track density profile vs. distance from the midrib, showing the region scanned, is illustrated in Figure 3. As will be discussed below, duplicate analyses were made in many cases and it is the average of the two analyses which is plotted. The error bars on the experimental data points are our best estimate of the overall error to be associated with a single measurement after compounding all measurement errors and errors associated with the background correction of the data. As with all errors quoted in this paper, the error bars in the figure are ± 1 standard deviation.

We first document the measurement errors, then discuss the background corrections and finally determine the overall error indicated in the figure.

A. Measurement Errors

Counting statistics errors ranged from 3-4%. All track density measurements were made by the same observer. However, even for a single observer, the consistency and reproducibility of the scanning over a period of several months is a very real concern, because the particle tracks registered in the lunar (vacuum) environment are small (up to $\sim$ 4 μ lengths, uncorrected for index of refraction), and the track densities are relatively low ($\sim 5 \times 10^3$ cm^{-2}). An advantage of Triafol TN is that, even after etching, the surface of the plastic is very smooth. Thus the majority of the etched features in the plastic detectors can be unmistakably classified as either tracks

or imperfections, but for every one hundred unquestionable cone-shaped tracks there were usually about a dozen questionable "pit" features that required a decision as to whether they were short tracks, tracks at near-vertical incidence, or just surface imperfections of the right geometry and diameter. The scanning criterion used was to decide between these alternatives on the basis of the contrast of the feature and the behavior of the image in focusing down into the plastic. In the scanning of each LNPE detector, separate tallies were made of: 1) the unmistakable tracks, 2) the questionable features which were most probably tracks, and 3) the questionable features which were not likely to be tracks. The track densities plotted in Figure 2 are those calculated from the sum of tallies 1) and 2), where typically tally 2) represents ~5% of the sum. Tally 3) was typically ~7% of the sum 1) + 2). Similar tallies made for high density ($\sim 10^5/cm^2$) samples yielded proportions of the 1) to 2) categories consistent with those observed for the lunar samples.

In an effort to maintain and monitor the consistency of the etching and scanning, control samples of the plastic were taken from the bulk roll, one adjacent to each detector used in the probe, and were all neutron-irradiated in contact with a boron target. Each control sample was etched and scanned along with its corresponding detector from the LNPE. The results of the control

measurements agree within counting statistics (± 3%). As will be discussed later, this provides only limited reassurance that a consistency in scanning was maintained since the track densities in the controls were a factor of 50-100 greater than the track densities in the LNPE detectors. However, the control sample results show that there is no evidence for significant variations in the registration efficiency of the plastic detectors over the rather large area of bulk plastic from which the LNPE detectors were taken. (In addition to the LNPE control samples two other series of measurements designed to test plastic uniformity show $\sim$ ± 3% variability for the portion of the roll used for the LNPE. Other portions of the roll show nonuniformity which could be as large as ± 5%.)

Replicate analyses were made of seven of the LNPE detectors in order to determine the reproducibility of the track density measurements. In most such "rescans," the identity of the sample was unknown to the scanner. From two to nine month intervals separated the initial and subsequent determinations. Taking into account the contribution to the total error from counting statistics, an average reproducibility of ± 5% was obtained with individual values ranging from 0-10%. No measurements were excluded in the data presented in Figure 2. It should be emphasized that different observers will in general not obtain the same results for these samples. Differences up to 10-30% can be expected.

Similarly, unless track counting is continued on a regular basis, a single observer cannot maintain completely consistent scanning criteria at these low densities.

A full evaluation of the errors in measurement requires consideration of the relative variations in the efficiencies of the boron targets which can result from: 1) variations in the thickness and quality of the vapor-deposited boron metal, and 2) small differences in the target-detector geometries. The thickness and uniformity of several of the targets were checked by alpha-backscattering techniques using the California Institute of Technology tandem Van de Graff accelerator. All targets examined, although not perfectly uniform, were "infinitely thick"; that is, they were all deposited to thicknesses, at all points on the target, which were greater than the range of the 1.5 MeV alpha particles emitted. In addition, each of the 23 targets used in the instrument was individually tested prior to its incorporation in the probe. A plastic detector was wrapped in direct contact over each target, and the targets were then irradiated in a Pu-Be neutron source. The total spread in the relative efficiencies obtained was $\pm$ 6½% of the mean, with a standard deviation of 3½%, which can be ascribed solely to counting statistics. The variation in target efficiencies due to variations in target-detector geometries was determined from

calibration irradiations, in which the probe was irradiated with fresh detectors in a uniform neutron flux (see paper I). Comparisons between targets (involving half the total number of targets) in four different irradiations yielded differences in track densities from 0-10% with a mean deviation of 4% (beyond that attributable to counting statistics). When applied to specific detector positions, there are no cases where variations observed in the calibration irradiations could be correlated with scatter in the lunar data (Figure 2). Thus, we conclude that the geometry variations are not reproducible when the probe is reassembled and that the above error estimate should be applied on a statistical basis rather than to specific detector positions.

Compounding all errors, 3½% from counting statistics, 5% from scanning reproducibility and 4% from geometry variations, we estimate the overall error in measurement to be ± 7%.

B. Background Corrections

The LNPE was only activated when deployed on the lunar surface, so background from neutron capture in the target occurring during the flight is not involved here. Contributions to the background from any fossil tracks (e.g., tracks from atmospheric radon decay) which had accumulated in the plastic prior to use in the LNPE were eliminated prior to the mission by an annealing at 115° C for 9 days. Residual track densities after this

annealing procedure are extremely low, $\sim 50/cm^2$.

A serious concern was the neutrons produced during the LNPE deployment by the power source (RTG) for the lunar surface geophysical experiments which, because of mission timeline requirements, was situated 35 meters away from the LNPE site. However, as discussed in detail in paper I, the background estimated both from a field simulation experiment and from theoretical considerations, is small (between $2\frac{1}{2}$ - 3%), even at depths where it is expected to have the largest effect.

The remaining sources of background include the direct registration of galactic cosmic ray ions (which is more important for the plastic detectors than the mica because they are more sensitive), the production of interaction tracks in the plastic due to high energy cosmic ray protons and alpha particles, and recoil tracks from the interaction of high energy (MeV) neutrons produced by the RTG during the flight to the moon. The total contribution from all these sources can be determined experimentally by track density measurements made in areas of the detectors never exposed to the targets, including regions behind the ribs of the rib cage and in an outer second layer of plastic wrapped over the rib cage windows (see Figure 1). No systematic position dependence of the background was observed, and in a total of 0.8 cm^2 scanned an average track density of $200 \pm 50/cm^2$ was

obtained, which is a 3% correction for the data at 140 g/cm^2 and a 6% correction for the deepest data point.

Appropriately compounding the error in this correction with the previous 7% error, then, we arrive at an overall error for a single measurement of from 7 - 9% (one standard deviation).

IV. Absolute Neutron Capture Rates and Neutron Densities

The measured track density, ρ, in the plastic detectors can be related to the ^{10}B capture rate, P, in captures per gram ^{10}B per sec:

$$f\rho = \varepsilon PT \qquad (1)$$

where T is the exposure time of the probe, ε (in g/cm^2) is a measure of the detection efficiency, and f is a self-shielding correction which, as defined, is a dimensionless constant ≥ 1. The self-shielding correction must be applied because the target materials in the neutron probe are strong neutron absorbers, which attenuate the neutron flux, and thus the measured track densities are low compared to the values they would assume in the absence of the probe.

A. Self-shielding Correction

We have estimated the self-shielding factor, f, using the method described in paper I in which f for the lunar spectrum is bracketed between measurements of f for a well-thermalized

flux and for a 1/E (E = neutron energy) spectrum. A test unit of the probe was constructed which had targets made from B of natural isotopic composition (~ 20% ^{10}B) in addition to the ^{10}B targets. Exposure of the test probe to a 1/E spectrum was accomplished by wrapping the unit in 0.45 mm of Cd. The ratio of the track density per ^{10}B atom in the natural B targets to that for the ^{10}B targets is equal to f_{10}/f_n, where 10 and n refer to the ^{10}B and natural boron targets, respectively. The thermal irradiation gave $f_{10}/f_n = 1.44 \pm .06$, whereas the exposure in the 1/E spectrum yielded $1.07 \pm .03$. Unlike the case for U, the self-shielding in a natural B target cannot be neglected (that is, f_n cannot be assumed to equal unity) for the thermal irradiation. However, the value of the lunar capture rate is comparatively insensitive to f_n because f_n enters into the calculation of both f and ϵ in equation 1 and errors in f_n tend to cancel. An error of x% in f_n produces an error of ~ (x/3)% in the lunar capture rate. Consequently, it is sufficiently accurate to estimate f_n theoretically. We have generalized the standard literature calculation of the self-shielding effect on the bulk (volume) activation of a foil (see, for example, Drowlers, 1970) to cover the case of the surface activity of the foil, as measured by a track detector. The actual hemicylindrical probe geometery is rather complicated; thus, we have calculated, as limiting cases,

the self-shielding factor for an infinite planar track detector and for a spherical shell detector. The planar case yields f_n = 1.12, which is a lower limit because all the neutrons in this case will pass through the B target only once, whereas some neutrons will pass twice in the actual hemicylindrical geometry. The spherical shell case gives f_n = 1.19, which is an upper limit because essentially all the neutrons will pass through the target twice in this case. The spherical shell calculation yields f_{10}/f_n = 1.41 for a thermal spectrum, in good agreement with the experimental value; consequently, we give this calculation more weight and adopt a value of f_n = 1.17 ± .02 for a thermal spectrum. For the 1/E spectrum, f_n can be taken as 1. Thus, the ^{10}B self-shielding for a thermalized spectrum is f_{10} = 1.44 X 1.17 = 1.68, whereas for a 1/E spectrum it is 1.07. Following the arguments in paper I the lunar self-shielding should lie between these values, and we adopt f = 1.37 ± .16. The range of 1.07 to 1.68 is comparatively large and constitutes the largest source of error for the experiment. The ± 0.16 error estimate was obtained by regarding the total spread between 1.07 and 1.68 as equivalent to ± 2 standard deviations; consequently ± 0.16 is our best estimate of the standard deviation and can be compounded with equivalent errors from other sources.

B. Detection Efficiency

For ideal track detectors and targets placed in contact

(2π geometry):

$$\varepsilon_{max} = \tfrac{1}{4} (R_{\alpha} + R_{Li}) \qquad (2)$$

where R_{α} and R_{Li} are the ranges in B metal of the alpha particle and ^{7}Li nucleus from ^{10}B neutron capture. In practice the measured efficiency will be less than that calculated by equation (2) because: (a) The B target thickness is larger than the alpha particle range, producing a continuous distribution of alpha particle energies from 0 up to 1.5 MeV. The ionization rate of some of the low energy particles will be insufficient to leave an etchable track (Fleischer et al. 1967), and some fraction of the etched tracks near zero length will not be counted. Also, tracks due to particles entering the detector surface at shallow angles will be lost during the etching process (Fleischer and Price 1964). (b) There is a gap of roughly 1.9 mm between the targets and detectors. (c) The targets may be porous, contain impurities, or have thin surface films which will lower the efficiency.

Figure 3 shows that, in the areas of the detector scanned, the track density profile in the angular direction, i.e., around the probe, is flat to better than ± 4%, indicating that a good approximation to 2π geometry is obtained in this region. Similar profiles as a function of position along the probe are also flat (to better than ±4 %,) as expected from the target-detector geometry. Thus, losses in efficiency due to the 1.9 mm gap appear to be less than 4%.

The discussion of intertarget efficiency in the section on measurement errors indicates that intertarget variability is at most ± 4%. However, systematic inefficiencies of the type outlined in (c) cannot be ruled out. No carbon impurities could be seen in the alpha back scattering measurements, although concentrations $\geq$ 5% would have been readily detected. Great care was taken to keep the B targets clean prior to and during assembly of the probe. A final swabbing with reagent grade acetone was performed after mounting. Residual films, as judged by hydrogen surface analysis (Leich et al. 1973), from acetone are remarkably small.

An experimental value for the efficiency was obtained by irradiating a calibration unit of the probe constructed with natural boron targets in a well-thermalized, uniform neutron flux, using gold foil activation to determine the thermal neutron density (I). (It was desirable to have the flux monitoring for the calibration irradiations carried out independent of track measurements.) The gold foils were calibrated against the NBS standard neutron source (Murphey and Caswell, 1970). All the ^{197}Au measurements were corrected for resonance neutron activation by Cd absorption measurements. Negligible errors are introduced in the neutron density measurements due to deviations of the ^{197}Au capture cross section from 1/v (v = neutron velocity) behavior in the neutron energy range below the Cd cutoff energy

(see, for example, Axton, 1970). The capture rate for the natural B was calculated from the measured thermal neutron density assuming a cross section for ^{10}B (n,α) of 3842 barns at 2200 m/sec neutron velocity (Meadows, 1971). The efficiency for this irradiation was then calculated using the measured track density from the natural B targets by means of equation 1, with $f_n = 1.17$ as disucssed in the previous section, yielding $\epsilon = 0.137 \pm .009$ mg/cm^2. However, there are systematic errors involved in this calibration which require that a correction factor be applied to this value before it is applicable to the LNPE exposure. These are discussed below.

The precision of our data due to scanning errors and non-uniformity in the plastic detectors was discussed in the section on measurement errors. However, there are three other sources of error affecting the absolute neutron densities which arise from the (sometimes exasperating) properties of plastic track detectors.

(a) As judged by the visual appearance of the tracks, the etching rate of the plastic exposed on the lunar surface was comparatively uniform; however, using the same etching times as for the lunar plastic, the plastic used for the calibration unit (although from the same batch) was distinctly overetched. Consequently, shorter etching times (3-4 instead of 4½ hours) were used for the calibration plastic. The etching times were adjusted for each sample until the visual appearance of the tracks matched

those observed on the lunar plastic. This procedure is somewhat subjective, but once a calibration sample was accepted for scanning, the resulting track density was accepted without any reevaluation of the suitability of the sample. The quoted efficiency is based on 4 calibration samples selected in this manner. The standard deviation of the track densities for these 4 samples was ± 5.7%, which is larger than expected from counting statistics and/or scanning reproducibility and is undoubtedly due to the variable etching rates observed for the calibration plastic. This is the dominant source of error in the efficiency although not for the experiment as a whole.

(b) The registration of low energy alpha tracks in our Triafol TN is different in vacuum than in air, with higher registration efficiency and better formed tracks in air compared to vacuum. This presumably reflects the critical role played by oxygen in track registration in plastics as documented by Crawford et al. (1968) and Monnin (1969). Between atmospheric pressure and about 10^{-1} Torr , there is a 12 ± 3% decrease in the registration efficiency. Consequently, all calibrations were done in vacuum. Exposure of the plastic to high pressure oxygen following ^{10}B alpha particle irradiation, but prior to etching, did not improve either the appearance of the tracks or the registration efficiency relative to air. Pressures up to 6000 psi for times

up to 10 days were used. Also, samples exposed at lower pressures ($\sim 10^{-7}$ Torr) show "aging" or "recovery" effects (Blanford et al. 1970) in that the track density, for fixed etching and scanning conditions, increases with time upon being stored following irradiation, with the amount of recovery depending on the ambient pressure during the irradiation. Because the calibration irradiations were performed in relatively bad vacuum (0.1 - 1 Torr) and the lunar samples exposed under very good vacuum conditions, comparative measurements were made of control samples of the actual LNPE plastic exposed in a uniform neutron flux at 1 and 10^{-7} Torr pressure. The 10^{-7} samples showed track densities which were about 15% less than the 1 mm samples when etched within 2 days of the irradiation; however, after three weeks' storage in the dark in air at room temperature, the track densities in three pairs of 1 and 10^{-7} mm samples were the same to within ± 3 %.

(c) The lunar track densities are $\sim 5 \times 10^3$ tracks/cm^2, whereas the calibration samples have $\sim 5 \times 10^5$ tracks/cm^2. This factor of 100 was necessary to obtain enough activity in indium foil monitors which were used in order to determine the relative fluence between the calibration irradiation of the probe and the irradiation of the gold foils. In order to check whether there was any systematic difference in track counting efficiency over the factor of 100 range in track density, strips of plastics

adjacent to those flown were exposed to pyrex targets in vacuum at two different reactor power levels to produce track densities corresponding to the lunar and calibration samples respectively. The relative fluences for the two irradiations were monitored by In foil activation.

It was found that the ratio of the scanning efficiency at low track density was 0.88 ± 0.07 of that at high track density. Thus, the appropriate value for ε to be used with our LNPE track densities in equation (1) is $\varepsilon = 0.88 \times 0.137 \times 10^{-3} = (0.120 \pm 0.013) \times 10^{-3}$ g/cm^2.

For comparison, the maximum efficiency, calcuated from equation (2) is 0.32 mg/cm^2. If only alpha particle tracks were being counted, the maximum efficiency would be 0.22 mg/cm^2. The reasons why the measured efficiency is so much less than either of these values are not completely understood. Recoil ^{7}Li ions of 0.86 MeV (the maximum energy of the ^{7}Li from ^{10}B neutron capture) obtained by scattering protons from a LiF target produce recognizable tracks for the etching conditions used for the LNPE plastic. However, in order to understand the low measured efficiency, we must assume that the overall efficiency for etching and counting ^{7}Li ions of this and lower energy must be quite low and also that many of the lower energy alpha tracks must be lost in the etching and scanning. (For example, 0.25 MeV alpha

particles do not produce recognizable tracks for our etching and scanning conditions.) Comparative exposures of Triafol TN and good quality cellulose nitrate (prepared by E. V. Benton) placed side by side against a boron target in vacuum showed that the track density in the TN was 0.7 of that in the cellulose nitrate. Thus, even if the cellulose nitrate is a perfect track detector, this experiment shows that the relatively low efficiency of the probe can be primarily ascribed to the relatively poorer registration efficiency of Triafol TN for ^{10}B n-capture products. (The TN was chosen for its greater resistance to annealing, which was a considerable worry for this experiment.)

C. Calculation of Capture Rate and Neutron Density

Using the efficiency and self-absorption values discussed above, the observed track densities can be used to calculate capture rates via equation (1). Adopting, as in paper I, an arbitrary reference depth of 150 g/cm^2, a ^{10}B capture rate of 467 ± 74 captures per second per gm ^{10}B is obtained. Because ^{10}B has an absorption cross section which is strictly proportional to 1/v, where v = neutron velocity, the capture rate can be directly converted to a neutron density of (9.2 ± 1.5) X 10^{-6} neutrons/cc. Either of these values can be used to renormalize the track density profile in Figure 1. Capture rate and neutron density are equivalent for ^{10}B and are used interchangeably in the following discussion.

V. Comparison with Theoretical Calculations

A. Depth Profiles

In our previous papers (I and II) we have shown that the LNPE data are in good accord with the LCH calculations for the case of an Apollo 11 composition (a good approximation for the Apollo 17 deep core) for a temperature of 200° K and for an exponential production profile ($e^{-x/165}$ where x is the depth in g/cm^2) of MeV neutrons. The MeV neutrons, following moderation and diffusion, are the source of the low energy neutrons which produce the ^{10}B and ^{235}U capture. However, because the various theoretical calculations in the literature do not give identical results, a more detailed comparison is warranted. The neutron density is independent of temperature; consequently, we focus on a consideration of alternative MeV neutron source profiles and also discuss calculations published by other groups.

In addition to the exponential case, LCH calculated capture rates for a MeV source neutron depth profile (modeled from the results of Monte Carlo calculations by Armstrong and Alsmiller, 1971), which was constant to a depth of 165 g/cm^2 and then decreased exponentially at greater depths. Physically, the MeV neutrons are produced primarily by the evaporation stage of higher energy ($\gtrsim$ 20 MeV) nuclear reactions and, because they are secondary

particles, they are expected to show a build up from the surface to a maximum and then to fall off at greater depths. (The effect of surface leakage during moderation converts the MeV neutron profile into the low energy neutron density profile measured by the LNPE.) Thus, the two MeV source profiles used by LCH represent extremes in the sense that the exponential case has too many neutrons close to the surface, whereas the "flat + exponential" case has the neutron production concentrated at larger depths. Figure 4a compares the LCH neutron density profiles for the two source profiles. Considering the extreme differences in the source profiles, the two curves in Figure 4a, although distinct, are remarkably similar. This is because the shape of the neutron density profile is determined primarily by surface leakage during the slow-down process. In Figures 4b and 4c we show the best fits (by eye) of the two profiles to the measured neutron densities. Only the magnitude of the theoretical profiles was varied; the depth scale was held fixed. With the rather large error bars associated with the data, neither of the profiles can be confidently eliminated. Nevertheless, the fit for the exponential source function appears better than for the flat + exponential, where the data fall consistently below the curve at shallower depths and consistently above at greater depths.

The ^{37}Ar data for the Apollo 16 and 17 deep core (Fireman

et al. 1974; Stoenner et al. 1974) define the MeV source neutron profile much better than our neutron density measurements because the ^{37}Ar is produced primarily by MeV neutrons reacting with ^{40}Ca. The ^{37}Ar production rate peaks at 30-50 g/cm^2. This implies that the peak in the MeV neutron production rate will be at even shallower depths because surface leakage will shift the peak in the ^{37}Ar capture rate to larger depths. Independent of any theoretical analysis, this indicates that the LCH exponential MeV neutron source profile is more realistic. Further, Kornblum et al. (1973) were able to fit the ^{37}Ar depth profile for the Apollo 16 deep core with the exponential source profile but not with the flat + exponential case. Thus it appears that the maximum in the MeV neutron production rate is comparatively close to the surface, probably within the outer 30 g/cm^2.

The LNPE neutron density profile can be compared with the "thermal neutron" ($E < 0.4$ eV) flux profile of Armstrong and Alsmiller. Their profiles do not fit the LNPE data nearly as well as that of LCH, most likely because their MeV neutron source function is close to the "flat + exponential" case in Figure 4a. Our comparisons have been made with the Armstrong-Alsmiller calculations for both solar and maximum and using the cases which included rare-earth absorption.

The ^{157}Gd depth profile calculated by Kornblum et al. (1973) would describe the LNPE neutron density data reasonably well except that this theoretical curve appears to peak somewhat too close to the surface. The neutron density and ^{157}Gd profiles of LCH are very similar.

We conclude that, of the various theoretical calculations, the shape of the LNPE neutron density profile is best reproduced by the LCH calculations for an exponential MeV neutron source profile.

Using the LCH neutron density profile as a basis for extrapolating, we can evaluate the neutron density at the lunar surface of $(0.72 \pm 0.11) \times 10^{-6}$ n/cc. The surface neutron density is important because it governs the yield of neutron capture gamma rays that were detected by the Apollo 15 and 16 orbital gamma ray experiment (Reedy et al. 1973). As with ^{10}B, the neutron capture cross section for elements lighter than iron varies as 1/v; thus, the LNPE ^{10}B capture rates per atom can be converted into capture rates for these elements by multiplying by the ratio of the standard 2200 m/s neutron capture cross section of that element to that of ^{10}B. This conversion is independent of any theoretical calculation and involves no additional error other than that in the LNPE data.

B. Comparison of Absolute Capture Rates

The LCH theoretical ^{10}B capture rate at 150 g/cm^2, when adjusted to correspond to the cosmic ray intensity during the Apollo 17 mission according to the methods described in paper I, is 575 captures per second per gram ^{10}B (using the exponential MeV neutron profile). Although this is higher than the measured capture rate of 467 $\pm$ 74, the agreement is satisfactory, particularly when the $\pm$ 30% uncertainty estimated by LCH for the normalization of the theoretical capture rate is considered. Direct comparison of absolute rates for the other theoretical calculations is not possible with results available to us at present.

In II we compared the LNPE capture rates and those of Co^{60} (Wahlen et al., 1973), ^{37}Ar (Fireman et al., 1973), and ^{236}U (Fields et al., 1973) data in lunar samples with the corresponding rates calculated by LCH. Even though the various reactions occur in different neutron energy ranges, all the experimental capture rates except that for ^{236}U appeared slightly low by about a constant factor (Figure 5). Figure 5 differs from figure 2 of paper II in that the final ^{10}B capture rate is slightly lower and the ^{37}Ar capture rate has been corrected (using methods described in I) for the difference in the galactic cosmic ray intensity between the period just prior to Apollo 16 and that for the average over the last solar cycle. Taking the range of overlap of the 1 standard deviation error bars of the experimental capture rates excluding ^{236}U (as discussed in II), we conclude that except at low ($\lesssim$ 0.5 eV) energies the best estimate of lunar neutron capture rates is made by taking 0.8 of the rate calculated by LCH. The situation at low energy is

discussed in the following section.

Capture rate of ^{157}Gd

In addition to the factor of 0.8 discussed above, there are two sets of data which indicate that the calculated LCH rate for ^{157}Gd neutron capture is high: (1) the measured ratio of the ^{149}Sm capture rate to that of ^{157}Gd is about 20% higher than that predicted by LCH (Russ et al., 1971; Russ 1973). The ^{149}Sm capture occurs primarily through a resonance at 0.1 eV, whereas the equivalent resonance for ^{157}Gd is at 0.3 eV. (2) The LNPE Cd absorption measurement (paper II) indicated that the ratio of the neutron density below 0.5 eV to that above was 1.1 ± 0.2 at 180 g/cm^2, whereas the LCH calculations gave 1.7. At 370 g/cm^2, however, the measured (1.9 ± 0.3) and calculated (1.9) ratios were in agreement. Both of these differences (1 and 2) are independent of the 0.8 renormalization discussed above. The ^{157}Gd capture rate for an Apollo 11 composition calculated by Kornblum and Fireman is $\sim$ 13% higher than LCH, and their Sm to Gd capture rate ratio is lower than LCH. Thus, revisions to the Kornblum-Fireman calculations are also indicated. The following discussion considers only the LCH calculations.

The LNPE ^{10}B and ^{235}U data show that the total neutron density, after renormalization , is in accord with LCH; only the distribution in neutron density above and below 0.5 eV is not correct. The sense of the difference is that there are too many neutrons below 0.5 eV in the theoretical spectrum. (The ^{235}U fission cross section is not exactly 1/v; however it is close enough that the fission rate is relatively insensitive to variations in the shape of the low energy spectrum provided the total neutron density is held fixed). Because the ^{149}Sm resonance is well

below 0.5 eV, it follows that, at least in the depth interval near the peak, both the ^{149}Sm and ^{157}Gd capture rates calculated by LCH are too high and, from item (1) above, that the ^{157}Gd rate is more off than that for ^{149}Sm. Thus, an additional correction is required to the ^{157}Gd capture rate which must be at least as large as the factor of 1.2 difference between the theoretical and measured relative ^{157}Gd and ^{149}Sm capture rates (item 1 above) and relative to the original LCH calculation, the ^{157}Gd capture rate should be lowered by at least a factor of $\sim 0.8/1.2 = 2/3$. Strictly speaking, this factor will apply only in the depth range 150-200 g/cm^2; but, since the capture rates are highest in this range, it is reasonable, in the absence of more refined calculations, to adopt this factor at all depths.

An actual estimate of the effect of deviations of the low energy spectral shape from that calculated by LCH can be made using the family of spectral shapes which were generated by LCH in order to explore the effect of variations in the average absorption cross section (Σ eff) on the calculated capture rates (see figure 5 of their paper). Higher absorption gives a harder low energy spectrum and thus gives: (1) a higher ratio of the ^{149}Sm to ^{157}Gd capture rates P_{149}/P_{157}, and (2) a lower ratio of neutron density below to above 0.5 eV. We have used the correlations (Fig. 6) between the calculated values of the parameters (1) and (2) and the ratio, (P_{157}/P_{10}), of the ^{157}Gd to ^{10}B capture rates for the above spectral shapes. From these correlations we interpolated P_{157}/P_{10} for values of (1) and (2) corresponding to the measured quantities. The interpolated values can then be combined with the measured ^{10}B capture rate to estimate the ^{157}Gd capture rate.

The correlation curves in Fig. 6 were generated by using neutron energy spectra obtained by varring the absorption cross section for temperatures of 0 and 400°. The absorption cross section and temperature have no physical significance in this calculation; they are just parameters which are used to define a systematically varring series of low energy neutron spectra which are used to fit the two experimental parameters defining the low energy spectra. The significant observation from Figure 6 is that small variations in the neutron density ratio or in the relative Sm to Gd capture rate imply relatively large variations in the ^{157}Gd capture rate. This is reasonable considering the very low energy (0.03 eV) of the ^{157}Gd capture resonance. Figure 6 also shows the experimental LNPE neutron density ratio and the Sm/Gd capture rate ratio for soil 10084 (chemically very similar to the Apollo 17 drill core soils) and the associated errors in these quantities. It can be seen from both Figs 6a and 6b that P_{157}/P_{10} ratios which are distinctly lower than those calculated by LCH (shown by the cross in the figure) are implied. Table 1 summarizes the interpolated relative ^{157}Gd to ^{10}B capture rates required to fit both the neutron density ratio and the Sm/Gd capture rate ratio for the 2 spectral families. Table 1 shows that consistent results are obtained for all four interpolations, indicating $P_{157}/P_{10} = 12 \pm 1.5$, compared to the LCH ratio of 18.8. Taking the "best" experimental value for the ^{10}B capture rate as 0.8 times the LCH value, we estimate that the ^{157}Gd capture rate is 12/18.8 x 0.8 = 0.51 of that calculated by LCH.

It is important that consistent ^{157}Gd capture rates are obtained from fitting both the neutron density ratio and the relative Sm to Gd capture rates because there are possible, although less probable, alternative explanations for the differences between theory and experiment. For example, as pointed out by Russ (1973b), different sets of ^{149}Sm resonance parameters than those used by LCH will give calculated relative Sm to Gd capture rates more in accord with experiment. It would probably be worthwhile to have additional measurements of the relative ^{149}Sm and ^{157}Gd cross sections in the thermal energy range. Also, it is conceivable that the LNPE Cd ratios are somewhat too low due to a hardening of the lunar low energy neutron spectrum by the presence of the probe itself. Such an effect is referred to as "flux depression" in the neutron physics literature and is distinct from the "self-shielding" corrections discussed above. However, the flux depression effects are less important and usually not considered in most practical applications (Drowlers, 1970). In any case it seems less likely that the LCH low energy spectrum is actually correct and that other effects have independently produced similar discrepancies between theory and experiment for both the Sm/Gd capture ratio and the neutron density ratio.

In summary, the above discussion indicates that the best estimate at present of the lunar ^{157}Gd capture rate is at least 0.7 and probably 0.5 of the rate calculated by LCH at all depths. This estimate is sufficiently uncertain that it would be worthwhile for additional theoretical calculations to be carried out to attempt to reproduce very closely the great variety of experimental data now available on lunar neutron capture.

Special emphasis, perhaps even including the effects of crystal binding (Williams 1966) should be given to calculating the low energy below 1 eV) spectrum. Except for quantities sensitive to the detailed shape of the low energy spectrum, the LCH calculations reproduce the experimental data admirably well; however the above discussion shows that the most important neutron capture rate (^{157}Gd) is rather sensitive to these differences, thus additional effort on the low energy region is warranted.

Experimentally, we believe that, with additional effort, it would be possible to reduce the errors on the LNPE data by about a factor of 2. We do not feel this effort is warranted at the present time; however the LNPE materials will be carefully preserved and documented in order that additional work on them will be possible. It should be emphaiszed (see discussion in WBI) that the largest source of error in both the ^{235}U and ^{10}B rates is in the self-shielding correction and arises because we have felt that it was important to quote experimental results which were completely independent of any theoretical calculation. If a specific form of the neutron energy spectrum is assumed, it should be possible to calculate the self-shielding factor more closely (or in principle to perform an irradiation in a simulated energy spectrum) and in this sense "reduce" the errors in the LNPE rates.

A lower ^{157}Gd capture rate will reduce, but probably not completely eliminate, the differences between the measured low energy neutron fluences in lunar soil samples and those calculated from the LCH capture rate assuming a uniformly mixed regolith. (See paper II for an extensive discussion of this problem).

In our previous papers (I and II) we interpreted the relatively good agreement between the LNPE data and the LCH calculations as indicating that the conclusions drawn previously from ^{157}Gd data in lunar samples using the LCH capture rates would not require revision. Although caveats were given about the sensitivity of the ^{157}Gd production rate to the detailed shape of the low energy spectrum, we did underestimate the sensitivity of the ^{157}Gd capture rate to relatively small differences in the measured Sm/Gd capture rate ratios and the LNPE Cd ratio with those calculated by LCH. We regard the proposed reduction in the ^{157}Gd capture rate to be a significant revision. In particular we propose that the ages and depositional time scales for the Apollo deep core samples (Russ et al., 1973; Russ 1973a, b) should be increased by a factor of 1.5 to 2.

The lower ^{157}Gd capture rate which we propose accentuates a problem pointed out by Russ (1973b) for rock 12002 in a detailed comparison of different neutron capture effects in lunar samples. For 12002 there exist excellent analytical data for ^{157}Gd and ^{131}Xe produced by ^{130}Ba neutron capture (Russ 1973, Marti and Lugimair 1971, Alexander 1971); however the amount of ^{157}Gd neutron capture was too large compared to that for ^{130}Ba. A lower ^{157}Gd capture rate makes the situation still worse and further attention must be given to the 12002 dilemma.

Acknowledgement

The successful mechanical design of the neutron probe is due primarily to the efforts of Curtis Bauman. The key to this phase of the experiment were the boron targets which were prepared under trying circumstances with unparalled dedication by Eileen Hess. We thank Richard Gomberg for aid with the self absroption calculations and Jeanne Grinols for typing every (expletive deleted) word of the LNPE. We have benefited from discussions with G. Price Russ, R. Lingenfelter, and D. Curtis. Finally, we gratefully acknowledge the support of the many branches of NASA which made the successful execution of the LNPE possible. This research was supported by NASA contracts NAS 9 12585 and NSG 07 023.

REFERENCES

Alexander, C. (1971), Spallogenic Ne, Kr, and Xe from a depth study in 12002, Proc. Second Lunar Sci. Conf., 2, 1651-1670.

Axton, E. J., (1970), Results of the intercomparisons of the thermal neutron flux density unit (1966-1968), Metrologia, 6, 25-32.

Blanford, G.E., Walker, R.M., and Wefel, J.P., (1970), Calibration of plastic track detectors for use in cosmic ray experiments, Radiation Effects 3,

Crawford, W. T., Desorbo, W., and Humphrey, J. S., (1968) Enhancement of track etching rates in plastics by a photo-oxidation effect. Nature, 220, 1313-14

Droulers, Y., (1970) in Neutron fluence measurements, Technical Report Series No. 107, IAEA, Vienna, pp. 52-58.

Eugster, O., Tera, F., Burnett, D. S., and Wasserburg, G.J. (1970) The isotopic composition of Gd and the neutron capture effects in samples from Apollo 11, Earth Planet. Sci. Lett. 8, 20-30.

Fields, P. R., Diamond, H., Metto, D. N., and Rokop, D. J. (1973) Reaction products of lunar uranium and cosmic rays. Proc. Fourth Lunar Sci. Conf., 2, 2123-2130.

Fireman, E., D'Amico, J., and DeFelice, J., (1973) Radioactivities vs. depth in Apollo 16 and 17 soil. Proc. Fourth Lunar Sci. Conf., 2, 2131-2145.

Fleischer, R.L., and Price, P.B., (1964) Glass Dating by Fission Fragment Tracks, J. Geophys. Res., 69, 331-9.

Fleischer, R. L., Price, P.B., Walker, R. M., and Hubbard, E. L., (1967) Criterion for registration in dielectric track detectors. Phys. Rev., 156, 353-5.

Kornblum, J.J., Fireman, E. L., Levine, M., and Aronson, A., (1973) Neutrons in the moon. Proc. Fourth Lunar Sci. Conf., 2, 2171-2182.

Leich, D.L., Tombrello, T. A., and Burnett, D. S., (1973) The depth distribution of hydrogen in lunar materials. Earth Planet. Sci. Lett., 19, 305-314.

Lingenfelter, R. E., Canfield, E. H., and Hampel, V. E., (1972) The lunar neutron flux revisited. Earth Planet. Sci. Lett. 16, 355-369.

Marti, K., and Lugmair, G. W. , (1971) Kr^{81}-Kr and K-Ar^{40} ages, cosmic-ray spallation products, and neutron cpautre effects in lunar samples from Oceanus Procellarum. Proc. Second Lunar Sci. Conf., 2, 1591-1605.

Meadows, J.W., (1971) Thermal neutron capture cross sections of ^{6}Li and ^{10}B by the pulsed neutron method, in Neutron Standards and Flux Normalization U.S.A.E.C., Symposium Series No. 23, (conf-701002), A. B. Smith ed., 129-135.

Monnin, M., (1969) Interaction des ions lourds avec des dielectriques organiques macromoleculaires. Contribution a 'etude des detectors solides de traces, Thesis, U de Clermont, France.

Murphey, W.M., and Caswell, R.S., (1970) Analysis of results of the Bureau International des Poids et Mesures thermal neutron density intercomparison, Metrologia, 6, 111-115.

Reedy, R.C., Arnold, J.R., and Trombka, J.I., (1973) Expected gamma ray emission spectra from the lunar surface as a function of chemical composition, J. Geophys. Res., 78, 5847-66.

Russ, G. P., III, Burnett D.S., and Wasserburg, G.J., (1972) Lunar neutron stratigraphy. Earth Planet. Sci. Lett., 15, 172-180.

Russ, G.P., III (1973a) Apollo 16 neutron stratigraphy. Earth Planet. Sci. Lett. 16, 275-289.

Russ, G.P., III (1973b) Thesis, California Institute of Technology.

Stoenner, R.W., and Davis, R. (1974) The fast neutron production of ^{37}Ar in the Apollo 17 deep drill string. In Lunar Science V, Lunar Science Institute, 741-743.

Wahlen, M., Finkel, R. L., Imamura, M., Kohl, C. P., and Arnold, J.R., (1973) ^{60}Co in lunar samples. Earth Planet Sci. Lett. 19, 315-320.

Williams, M.M.R., (1966) The slowing down and thermalization of neutrons, N. Holland, Chapter 3.

Woolum, D.S., Burnett, D.S., and Bauman, C.A., (1973) The Apollo 17 lunar neutron probe experiment. In Apollo 17 Prelim. Science Report, NASA SP-330, 18-1–18-12.

Woolum, D.S., and Burnett, D.S., (1974a) In-situ measurement of the rate of ^{235}U fission induced by lunar neutrons. Earth Planet. Sci. Lett. 21, 153-163. (Referred to as paper I in text).

Woolum, D.S., and Burnett D.S., (1974b) Lunar neutron capture as a tracer for regolith dynamics. To appear in Proc. Fifth Lunar Sci. Conf., 2, 2061-2074. (Referred to as paper II in text).

TABLE 1

Relative production rates of ^{157}Gd and ^{10}B*

	Spectral Family (Fig. 5)	
	T = 0	T = 400
Experimental		
Quality fit P_{149}/P_{157}	10.8 ± 1.3	13.0 ± 1.6
Neutron density below 0.5 eV / Neutron density above 0.5 eV	13.5 ± 2.3	11.4 ± 2.1
Theoretical		
LCH**	18.8	

*Production rates per target atom

**Calculation for Apollo 11 composition, 200°K, and depth averaged energy spectrum.

FIGURE CAPTIONS

Fig. 1. Schematic cross-sectional view of neutron probe across detector position not containing ^{235}U target. The rib cage is a frame assembly around which the plastic track detectors were wrapped. It could be rotated about the central rod containing the ^{10}B targets leading to ON and OFF configurations. The indicated areas of the plastic in which the ^{10}B alpha particle tracks were counted started 3 mm from the central mid rib and were 5 mm wide. The diameter of the central rod is 12 mm and the gap between the plastic and B target is 1.9 mm.

Fig. 2. Measured track densities from ^{10}B neutron capture as a function of depth beneath the lunar surface. The error bars include all sources of measurement error which affect the precision of a single measurement (see text).

Fig. 3. Sample track density (arbitrary units) profile in angular direction around probe (Fig. 1) showing that track density is flat in the actual range scanned for lunar data. Data obtained from calibration irradiation of flight unit.

Fig. 4. A. Comparison of neutron density profiles calculated by LCH for two different MeV neutron source profiles (see text). B and C. Comparison of LNPE data with shape of LCH density profiles shown in A. It is seen that the exponential profile (B) describes the LNPE data somewhat better. Only the vertical scale of the LCH profiles have been normalized to obtain a best fit in each case. No adjustment of the depth scales of the theoretical profiles has been made.

Fig. 5. The figure displays the ratio of the experimental neutron reaction rate to that calculated theoretically (LCH). For the LNPE data (^{235}U fission and ^{10}B) the symbols denote the targets for the reaction, whereas for lunar sample data the induced radiocativity is denoted by the symbol: ^{60}Co (Wahlen et al., 1973), ^{37}Ar (Kornblum et al., 1973), ^{236}U (Fields et al., 1973). The arrow in the ^{236}U position indicates that the measured ^{236}U decay rate is at least twice that calculated theoretically. The agreement between theory and experiment is good overall.

Fig. 6. Correlation curves for the calculated ratio of the ^{149}Sm to ^{157}Gd capture rates (P_{149}/P_{157}) and the ratio of neutron density below and above 0.5 eV vs. the ratio of the ^{157}Gd to the ^{10}B capture rate (P_{157}/P_{10}) for various theoretical low energy neutron spectra taken from LCH. Two family of spectra were used, parameterized by T = 0 and T = 400. For each family the spectrum was systematically varried to give the observed correlation lines. The hatchured regions show the experimental values for the quantities on the ordinates. The intersections of the curves and the experimental values correspond to neutron energy spectra which fit the experimental data. These interesctions correspond to P_{157}/P_{10} values that are distinctly lower than those calculated by LCH (indicated by crosses in the figure).

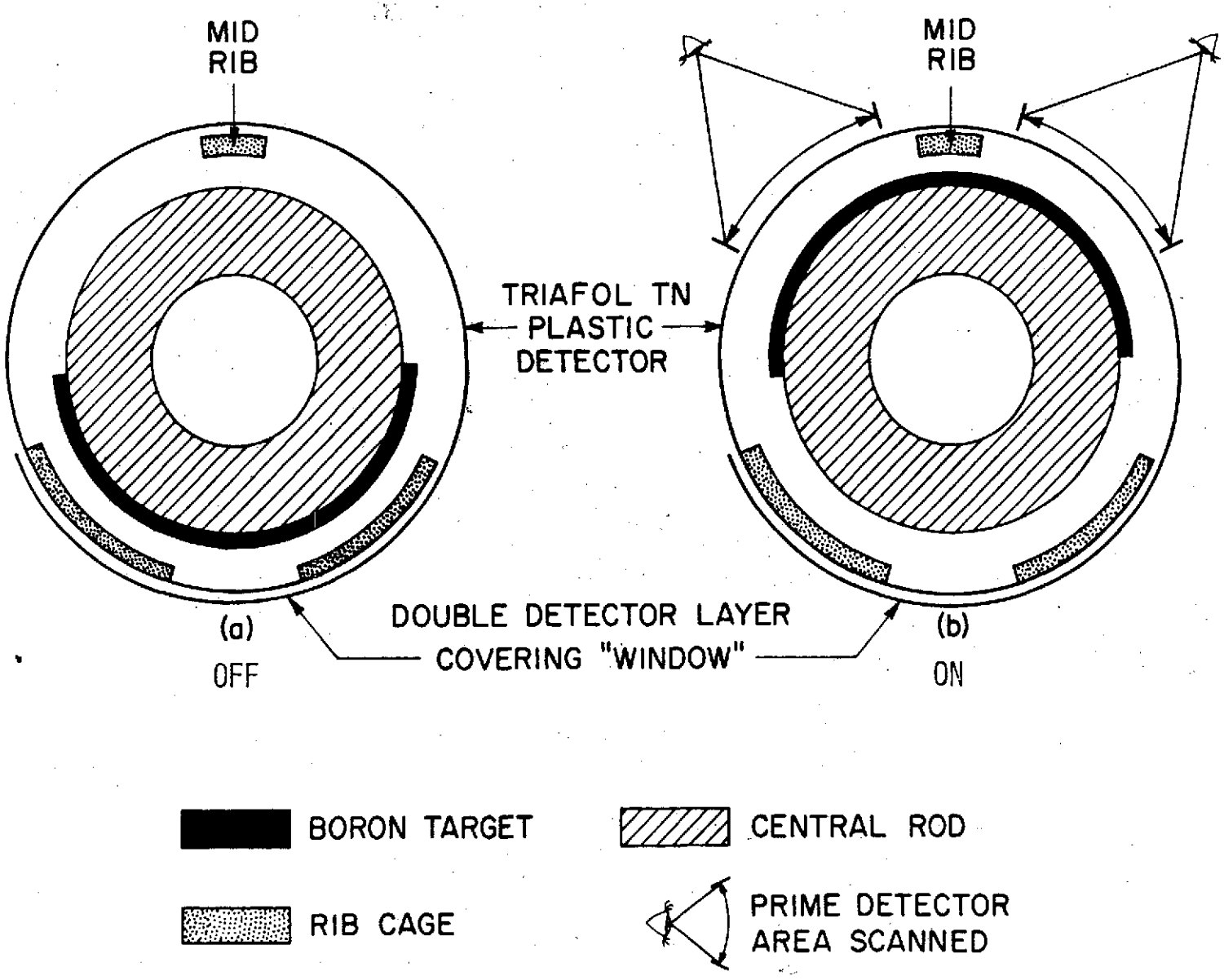
MID
RIB
MID
RIB
TRIAFOL TN
PLASTIC
DETECTOR
DOUBLE DETECTOR LAYER
COVERING "WINDOW"
(a)
OFF
(b)
ON
BORON TARGET
CENTRAL ROD
RIB CAGE
PRIME DETECTOR
AREA SCANNED

FIGURE 1

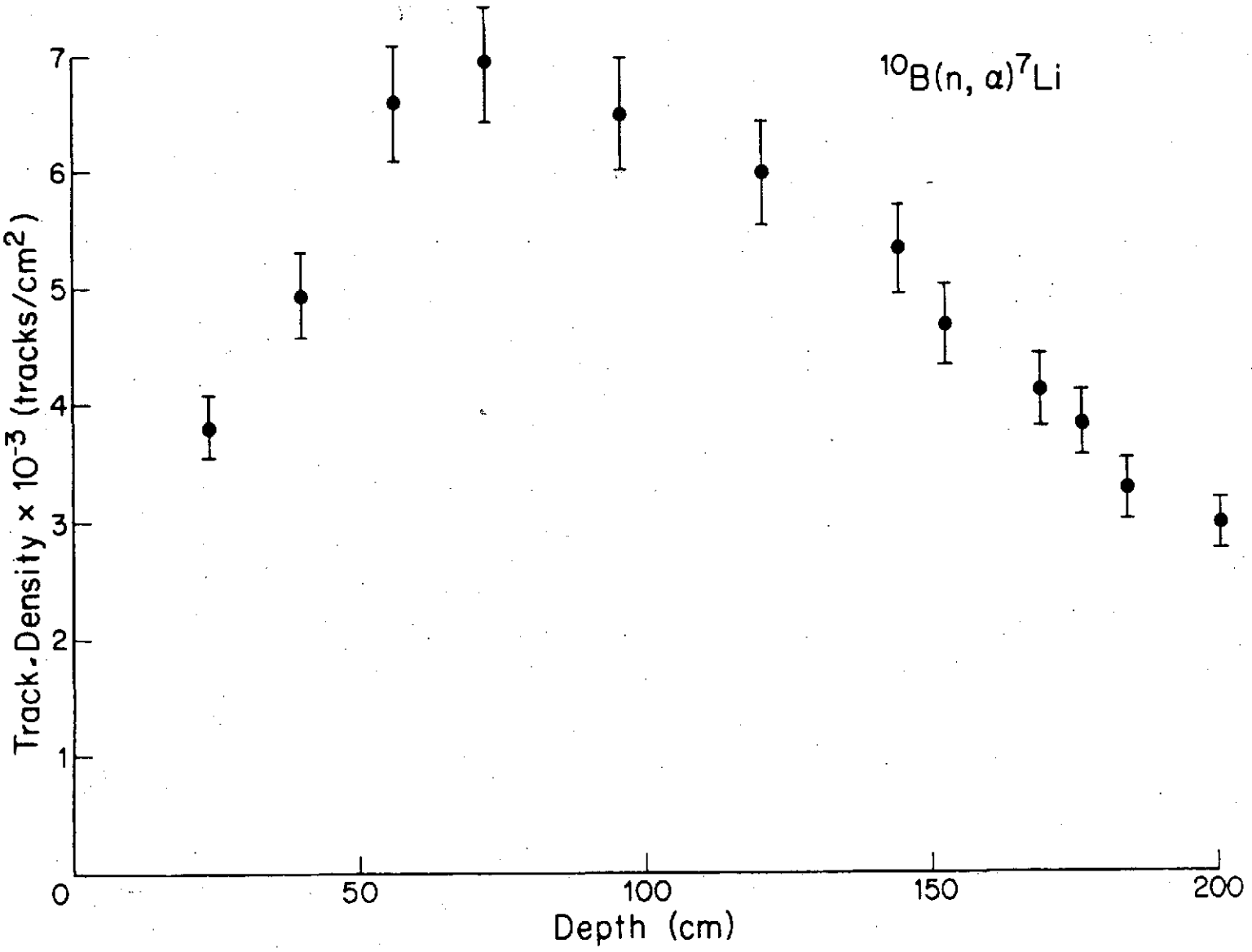
$^{10}B(n, \alpha)^{7}Li$
Track-Density x 10^{-3} (tracks/cm^2)
0
1
2
3
4
5
6
7
0
50
100
150
200
Depth (cm)

FIGURE 2

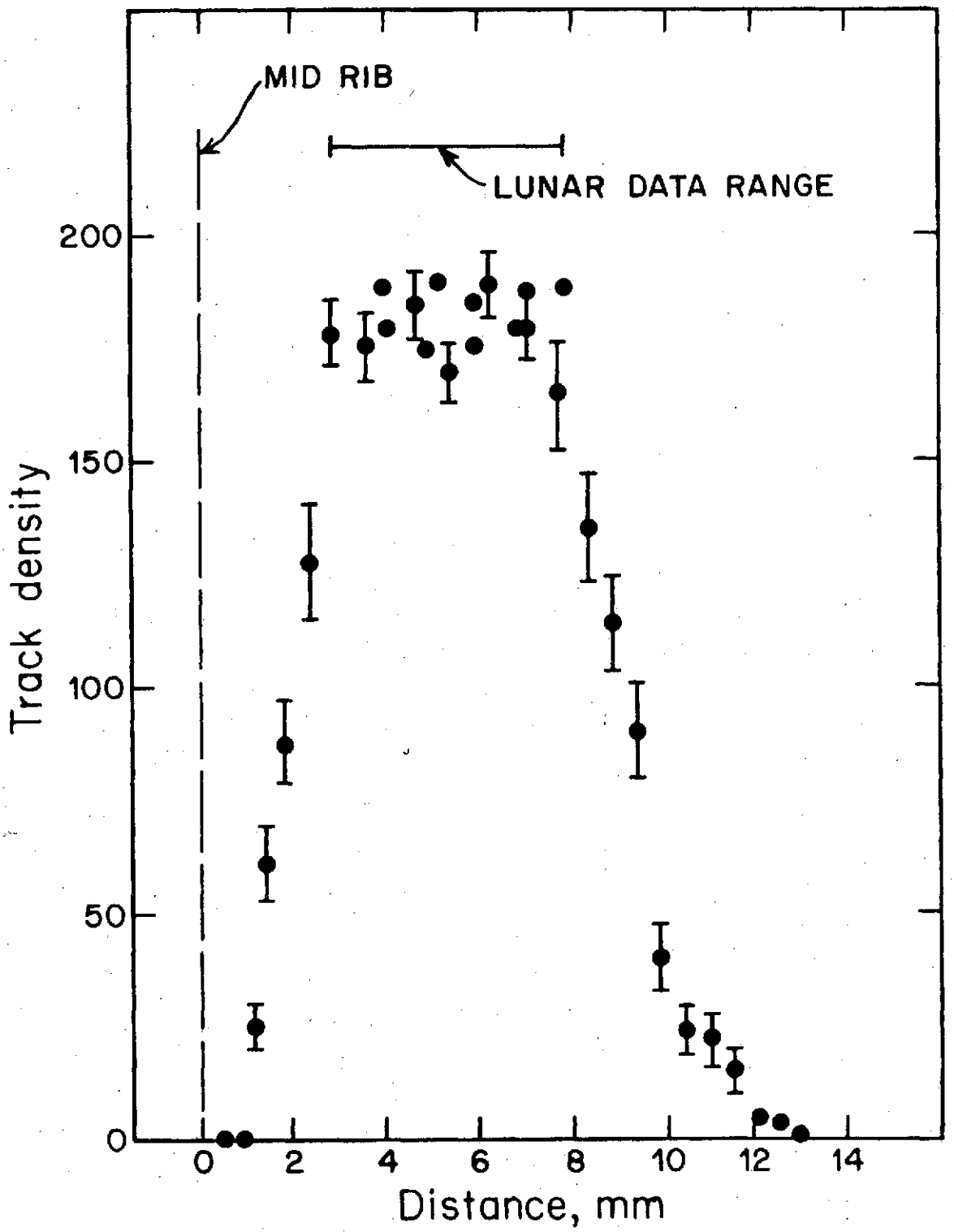
MID RIB
LUNAR DATA RANGE
Track density
200
150
100
50
0
0
2
4
6
8
10
12
14
Distance, mm

FIGURE 3

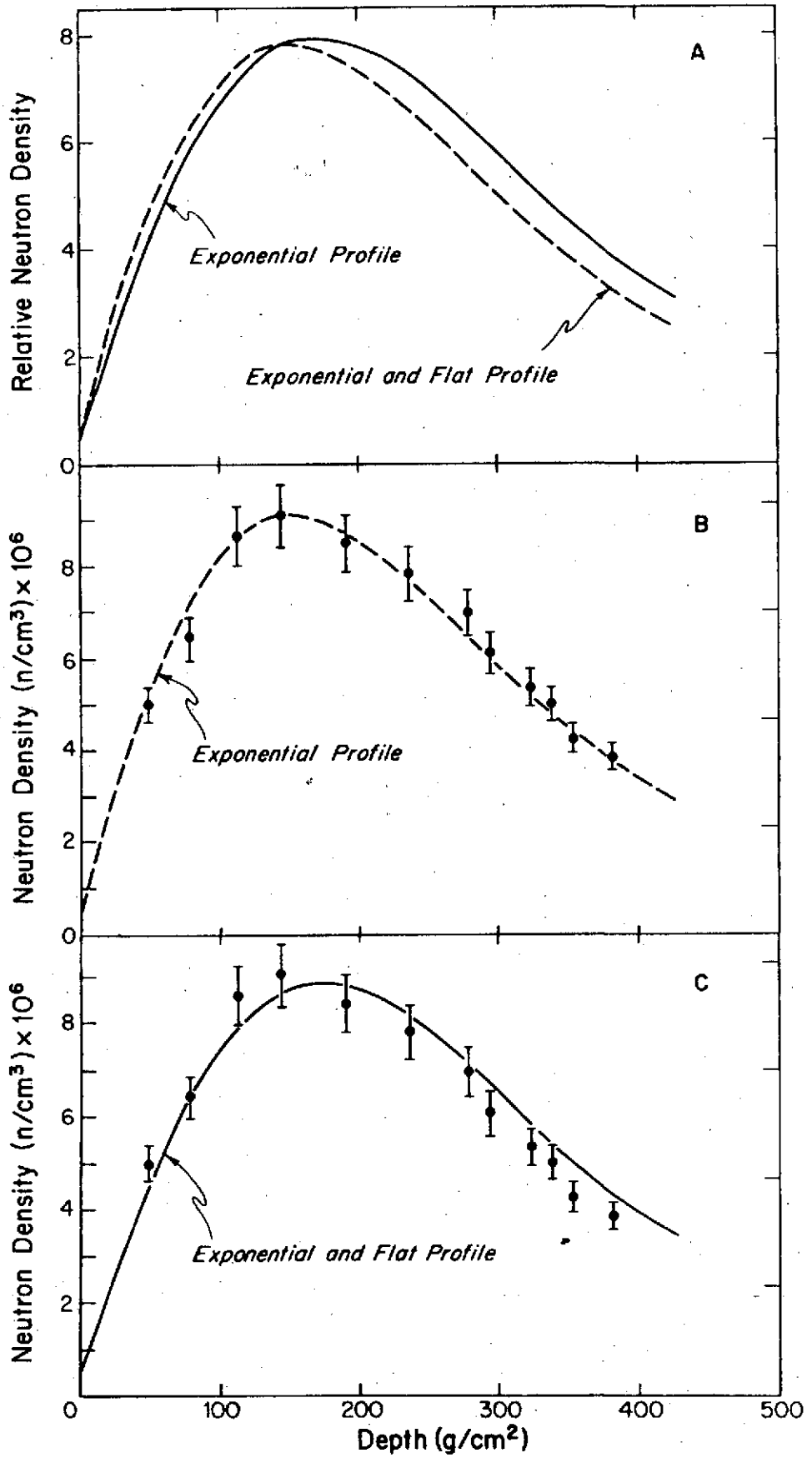
A
Relative Neutron Density
Exponential Profile
Exponential and Flat Profile
B
Neutron Density (n/cm³) x 10⁶
Exponential Profile
C
Neutron Density (n/cm³) x 10⁶
Exponential and Flat Profile
0
2
4
6
8
100
200
300
400
500
Depth (g/cm²)

FIGURE 4

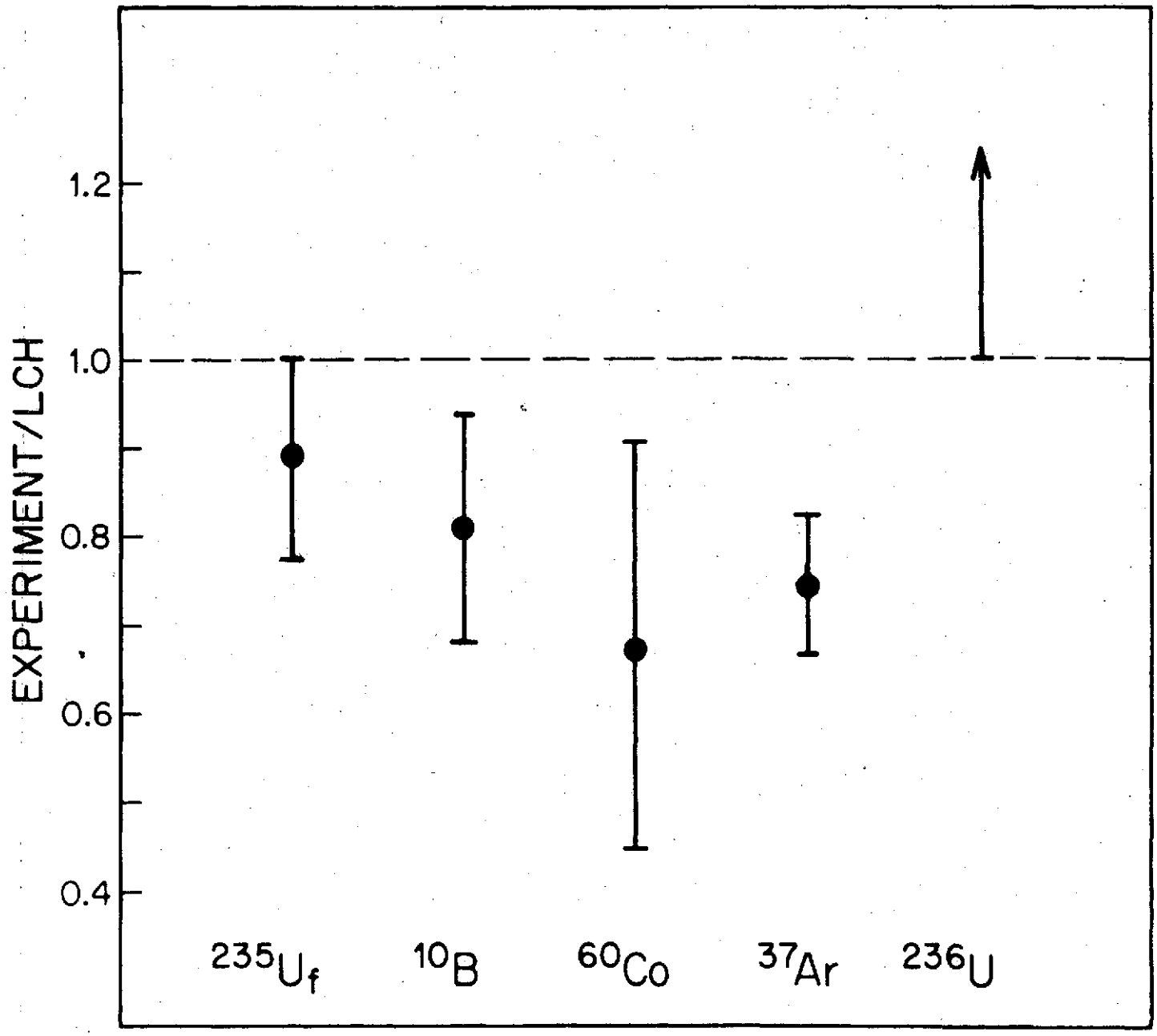

FIGURE 5

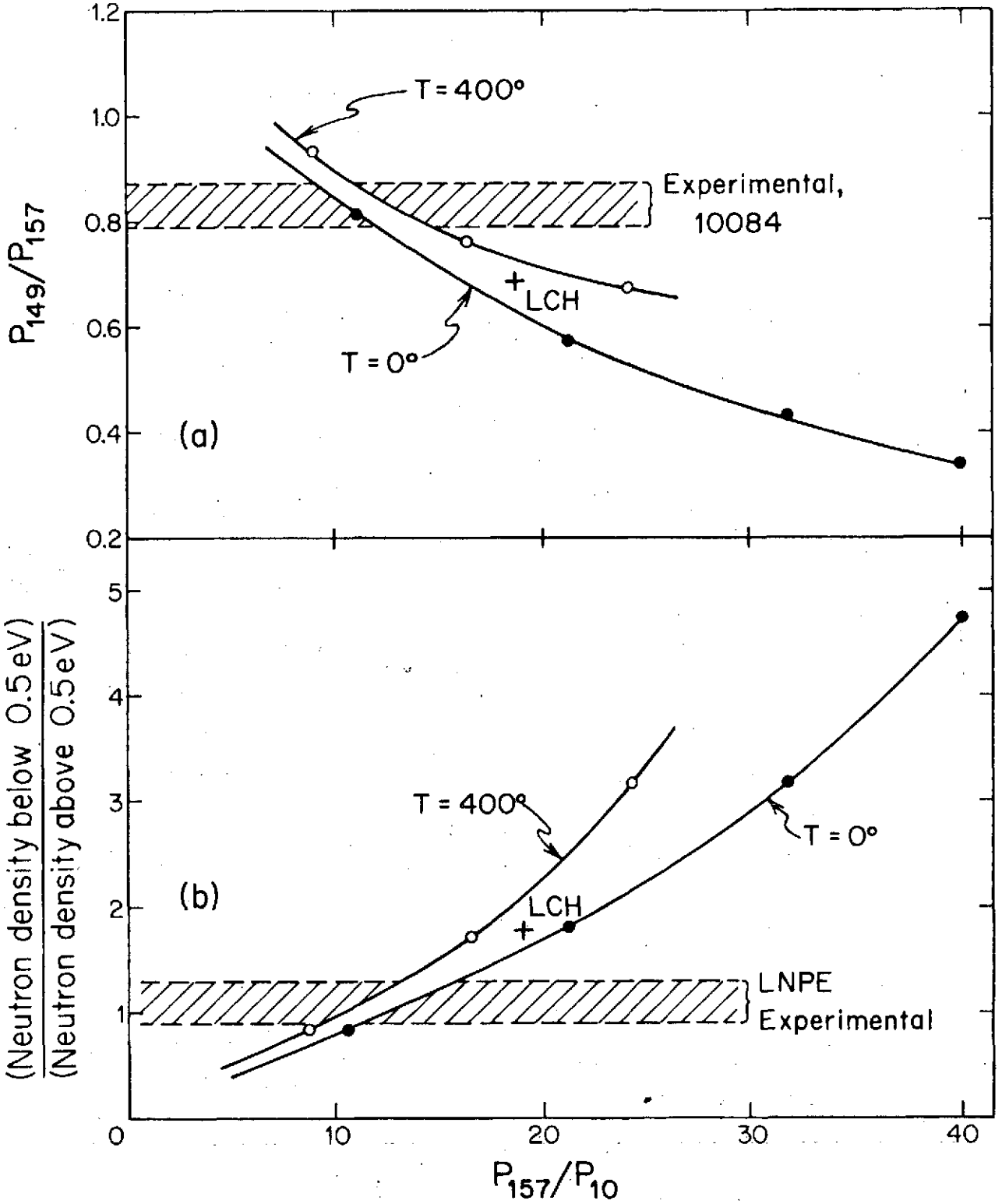
1.2
1.0
0.8
0.6
0.4
0.2
P_{149}/P_{157}
T = 400°
Experimental,
10084
+ LCH
T = 0°
(a)
5
4
3
2
1
0
(Neutron density below 0.5 eV)
(Neutron density above 0.5 eV)
T = 400°
T = 0°
(b)
LCH
+
LNPE
Experimental
10
20
30
40
P_{157}/P_{10}

FIGURE 6